Supplemental Material for "Anomalous non-Hermitian skin effect: the topological inequivalence of skin modes versus point gap"

Gang-Feng Guo,[1] Xi-Xi Bao,[1] Han-Jie Zhu,[2] Xiao-Ming Zhao,[3] Lin Zhuang,[4] Lei Tan,[1,5,*] and Wu-Ming Liu[2,†]

[1]*Lanzhou Center for Theoretical Physics, Key Laboratory of Theoretical Physics of Gansu Province, Lanzhou University, Lanzhou 730000, China*
[2]*Beijing National Laboratory for Condensed Matter Physics, Institute of Physics, Chinese Academy of Sciences, Beijing 100190, China*
[3]*Department of Physics and Institute of Theoretical Physics, University of Science and Technology Beijing, Beijing 100083, China*
[4]*State Key Laboratory of Optoelectronic Materials and Technologies, School of Physics, Sun Yat-Sen University, Guangzhou 510275, China*
[5]*Key Laboratory for Magnetism and Magnetic Materials of the Ministry of Education, Lanzhou University, Lanzhou 730000, China*

Contents

I: The derivation of the characteristic polynomial

In this section of the supplementary material, we present the details of the characteristic polynomial of the non-Hermitian three-band system. The Hamiltonian in real space is

$$H = \sum_{n=1}^{N} \Big[t_a {C^\dagger}_{A,n+1} C_{A,n} + t_c {C^\dagger}_{C,n} C_{C,n+1} + t_b ({C^\dagger}_{B,n} C_{B,n+1} + {C^\dagger}_{B,n+1} C_{B,n}) + \gamma_1 {C^\dagger}_{A,n} C_{B,n} + \gamma_2 {C^\dagger}_{B,n} C_{A,n} + \gamma_3 {C^\dagger}_{B,n} C_{C,n} + \gamma_4 {C^\dagger}_{C,n} C_{B,n} + V_a {C^\dagger}_{A,n} C_{A,n} + V_b {C^\dagger}_{B,n} C_{B,n} + V_c {C^\dagger}_{C,n} C_{C,n} \Big], \tag{S1}$$

where ${C^\dagger}_{A,n}$ ($C_{A,n}$), ${C^\dagger}_{B,n}$ ($C_{B,n}$) and ${C^\dagger}_{C,n}$ ($C_{C,n}$) represent the creation (annihilation) operators for sublattice A, B and C in n-th unit cells. t_a (t_b, t_c) is the hopping amplitudes and V_a (V_b, V_c) denotes the on-site potential for the the sub-chain A (B, C). γ_1 and γ_2 are hopping parameters between A and B sub-chain. Similarly, γ_3 and γ_4 are hopping parameters between B and C sub-chain. Without loss of generality, all parameters are taken as real numbers.

Due to the space translational symmetry, we can rewrite the Hamiltonian (S1) in the momentum space through the Fourier transform as

$$H(\beta)=\begin{pmatrix} \frac{t_a}{\beta}+V_a & \gamma_1 & 0 \\ \gamma_2 & t_b(\beta+\frac{1}{\beta})+V_b & \gamma_3 \\ 0 & \gamma_4 & t_c\beta+V_c \end{pmatrix}, \tag{S2}$$

where $H(\beta)$ is the counterpart of the Bloch Hamiltonian $H(k)$ via replacing $e^{ik}\to\beta$, $k\in\mathbb{C}$. Therefore, the characteristic polynomial of our system is

$$f(\beta,E)=\det[H(\beta)-E]=a_2\beta^2+a_1\beta^1+a_0\beta^0+a_{-1}\beta^{-1}+a_{-2}\beta^{-2}=0, \tag{S3}$$

with

$$a_2=-Et_bt_c+t_bt_cV_a, \tag{S4}$$

$$a_{-2}=-Et_at_b+t_at_bV_c, \tag{S5}$$

$$a_1=(t_b+t_c)E^2-(t_bV_a+t_cV_a+t_cV_b+t_bV_c)E+t_at_bt_c+t_cV_aV_b+t_bV_aV_c-\gamma_1\gamma_2t_c, \tag{S6}$$

$$a_{-1}=(t_a+t_b)E^2-(t_bV_a+t_aV_b+t_aV_c+t_bV_c)E+t_at_bt_c+t_bV_aV_c+t_aV_bV_c-\gamma_3\gamma_4t_a, \tag{S7}$$

and

$$\begin{aligned}a_0=&-E^3+(V_a+V_b+V_c)E^2+(\gamma_1\gamma_2+\gamma_3\gamma_4-t_at_b-t_at_c-t_bt_c-V_aV_b-V_aV_c-V_bV_c)E+t_bt_cV_a+t_at_cV_b\\&+t_at_bV_c+V_aV_bV_c-\gamma_3\gamma_4V_a-\gamma_1\gamma_2V_c.\end{aligned} \tag{S8}$$

The non-Bloch band theory can be articulated in Fig. S1 briefly. In Fig. S1(a), it can be found that the energy structure under different boundary conditions has tremendous deviations, which is caused by the non-Hermitian skin effect, i.e., the majority of eigenstates are pinned at the boundaries of the system [1], as shown in Fig. S1(b). To solve the distinction of the spectra, the concept of the generalized Brillouin zone and the corresponding continuum bands have been put forward [1, 2]. For our system, the generalized Brillouin zone and the corresponding continuum bands should be determined by $|\beta_2|=|\beta_3|$ due to the existence of a_{-2} [1, 2]. In Fig. S1(c), the generalized Brillouin zone and Brillouin zone are exhibited at the same time. Importantly, the distinction between them marks the occurrence of the non-Hermitian skin effect. As shown in Fig. S1(d), the continuum bands, obtained from the generalized Brillouin zone, can reproduce the open boundary eigenvalues perfectly. Here, we should emphasize that the condition of obtaining the generalized Brillouin zone, and the continuum bands, has nothing to do with γ_i $(i=1,2,3,4)$.

Further, when the conditions $V_a=V_c=V_{ac}$, $t_a=t_c=t_{ac}$ and $\gamma_1\gamma_2=\gamma_3\gamma_4$ are satisfied, the coefficients of the characteristic polynomial $f(\beta,E)$ can be simplified as

$$a_2=a_{-2}=-t_bt_{ac}E+t_bt_{ac}V_{ac}, \tag{S9}$$

$$a_1=a_{-1}=(t_b+t_{ac})E^2-(t_{ac}V_{ac}+2t_bV_{ac}+t_{ac}V_b)E+t_{ac}^2t_b+t_bV_{ac}^2+t_{ac}V_{ac}V_b-\gamma_3\gamma_4t_{ac}, \tag{S10}$$

$$a_0=-E^3+(2V_{ac}+V_b)E^2+(2\gamma_3\gamma_4-t_{ac}^2-2t_{ac}t_b-V_{ac}^2-2V_{ac}V_b)E+2t_{ac}t_bV_{ac}+t_{ac}^2V_b+V_{ac}^2V_b-2\gamma_3\gamma_4V_{ac}. \tag{S11}$$

One can see that the solutions satisfy

$$\beta_1=1/\beta_4,\beta_2=1/\beta_3, \tag{S12}$$

because Eq. (S3) is a reciprocal equation for β, which means that the generalized Brillouin zone is a unit circle exactly, as shown in Fig. S2(a). Physically, due to the generalized Brillouin zone consistent with the Brillouin zone, the eigenvalues between the open boundary and periodic boundary conditions, and the continuum bands match well with each other, as shown in Fig. S2(b). Moreover, the non-Hermitian skin effect, as we expected, is inhibited to appear in Figs. S2(c) and S2(d).

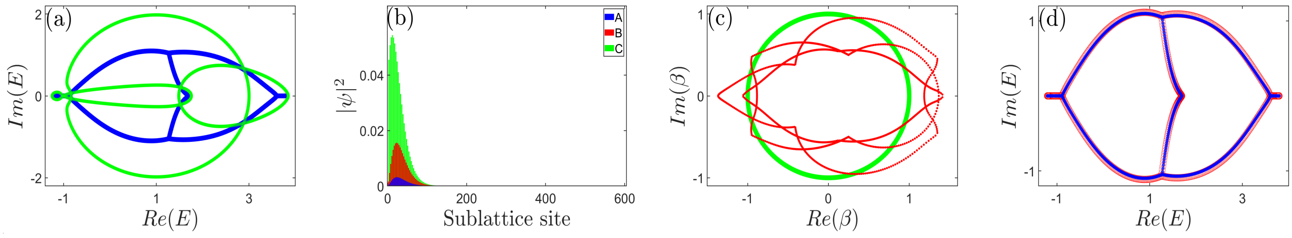

FIG. S1: (a) The eigenvalues under open boundary (the blue curve) and periodic boundary conditions (the green curve). (b) The non-Hermitian skin effect. (c) The generalized Brillouin zone (the red curve) and Brillouin zone (the green curve). (d) The open boundary energy spectrum (the blue curve) and the continuum bands (the red curve). The parameters are $N = 200$, $t_a = 1$, $t_b = \frac{4}{5}$, $t_c = 2$, $\gamma_1 = \gamma_2 = 1$, $\gamma_3 = \frac{1}{10}$, $\gamma_4 = \frac{1}{2}$, $V_a = 2$, $V_b = V_c = 1$.

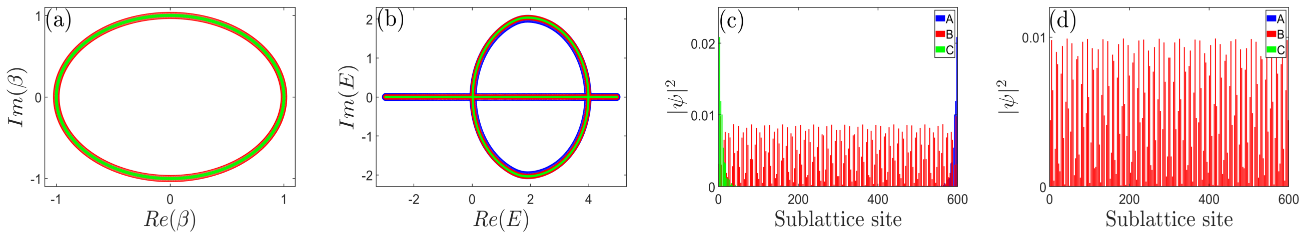

FIG. S2: (a) The generalized Brillouin zone (the red curve) and Brillouin zone (the green curve). (b) The eigenvalues obtained from the open boundary (the blue curve) and periodic boundary conditions (the green curve) and continuum bands (the red curve). (c) and (d) The distribution of the open boundary eigenstate. The parameters are $N = 200$, $t_a = t_c = 2$, $t_b = -2$, $\gamma_1 = -\gamma_4 = \frac{1}{4}$, $\gamma_2 = -\gamma_3 = -\frac{1}{3}$, $V_a = V_c = 2$ and $V_b = 1$, satisfying that Eq. (S3) is a reciprocal equation for β.

II: The analytic solutions in an open chain

A: The distribution of the open boundary eigenstates

We first consider the situation where one of the elements of the set $\{\gamma_1, \gamma_2, \gamma_3, \gamma_4\}$ is zero. Such as, we set $\gamma_1 = 0$. The Schrödinger equation $H|\Psi\rangle = E|\Psi\rangle$ for the open boundary Hamiltonian (S1) has the form

$$(H_{OBC} - E_{OBC}; N \times N)|\Psi\rangle = 0 =$$

$$\begin{pmatrix} V_a - E_{OBC} & 0 & 0 & 0 & \cdots & 0 & 0 & 0 \\ \gamma_2 & V_b - E_{OBC} & \gamma_3 & 0 & \cdots & 0 & 0 & 0 \\ 0 & \gamma_4 & V_c - E_{OBC} & 0 & \cdots & 0 & 0 & 0 \\ t_a & 0 & 0 & V_a - E_{OBC} & \cdots & 0 & 0 & 0 \\ \cdot & \cdot & \cdot & \cdot & \cdots & \cdot & \cdot & \cdot \\ \cdot & \cdot & \cdot & \cdot & \cdots & \cdot & \cdot & \cdot \\ \cdot & \cdot & \cdot & \cdot & \cdots & \cdot & \cdot & \cdot \\ 0 & 0 & 0 & 0 & \cdots & V_a - E_{OBC} & 0 & 0 \\ 0 & 0 & 0 & 0 & \cdots & \gamma_2 & V_b - E_{OBC} & \gamma_3 \\ 0 & 0 & 0 & 0 & \cdots & 0 & \gamma_4 & V_c - E_{OBC} \end{pmatrix} \begin{pmatrix} \Psi_{A,1} \\ \Psi_{B,1} \\ \Psi_{C,1} \\ \Psi_{A,2} \\ \cdot \\ \cdot \\ \cdot \\ \Psi_{A,N} \\ \Psi_{B,N} \\ \Psi_{C,N} \end{pmatrix}, \tag{S13}$$

with N being the total number of unit cells of the system, and $|\Psi\rangle$=($\Psi_{A,1}$, $\Psi_{B,1}$, $\Psi_{C,1}$, $\Psi_{A,2}$, ..., $\Psi_{A,N}$, $\Psi_{B,N}$, $\Psi_{C,N})^T$. Spectacularly, we can find that the Schrödinger equation $H|\Psi\rangle = E_{OBC}|\Psi\rangle$ in A sub-chain is

$$(V_a - E_{OBC})\Psi_{A,1} = 0, \tag{S14}$$

and

$$t_a\Psi_{A,i} + (V_a - E_{OBC})\Psi_{A,i+1} = 0, \tag{S15}$$

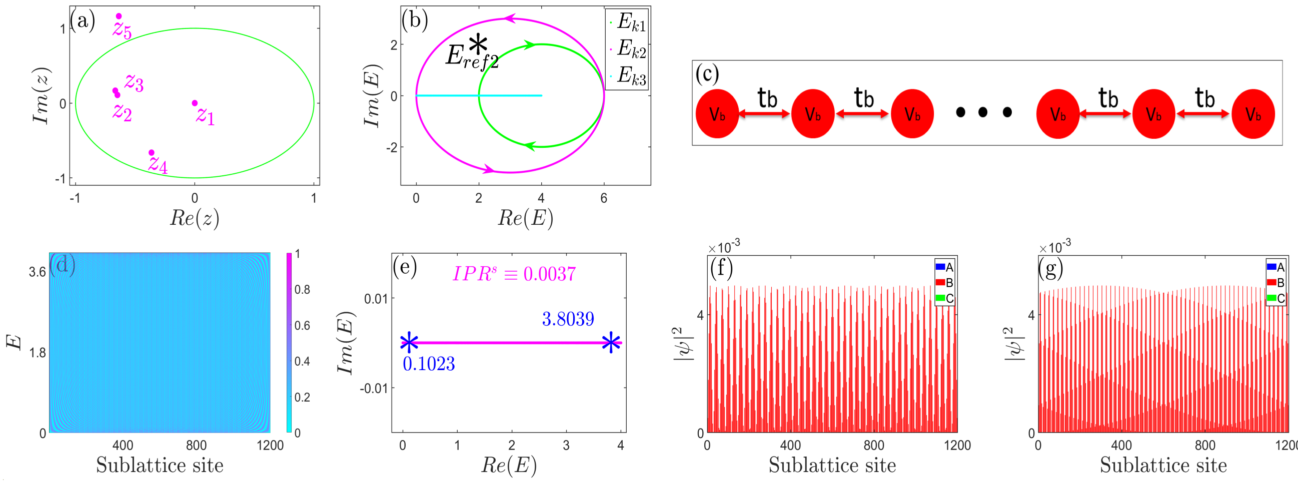

FIG. S3: (a) The distribution of the poles about the spectral winding $W = 1$ for $E_{ref1} = 1 + \frac{1}{2}i$ on the complex plane, in which z_1, z_2, z_3 and z_4 are encircled by the unit circle, while z_5 is outside the unit circle. (b) The nonzero spectral winding for $E_{ref2} = 2 + 2i$ obtained from (Re[det[H(k)]], Im[det[H(k)]]) as k varies from 0 to 2π. (c) Schematic representation of the Hermitian Hamiltonian H_B. (d) The normalized eigenstates with the change of eigenvalues, all of which are extended under open boundary conditions. (e) The open boundary eigenvalues colored by their IPR^s, which is a constant closing to zero. (f) and (g) The distribution of the eigenstates, corresponding to two eigenvalues in (e). The common parameters are $N = 400$, $\gamma_1 = \gamma_4 = 0$, $t_a = 2$, $t_b = 1$, $t_c = 3$, $\gamma_2 = \frac{1}{2}$, $\gamma_3 = \frac{1}{3}$, $V_a = 4$, $V_b = 2$ and $V_c = 3$.

with $i = 1, 2, ..., N-1$. The recurrence relation unambiguously shows that $\Psi_{A,j} = 0$ with $j = 1, 2, ..., N-1, N$ when $E_{OBC} \neq 0$, i.e., there is no probability distribution on the A sub-chain. Here, it should be emphasized that this conclusion is one of the essential parts of this work, as we will explain below. Similar result of $\Psi_{C,j} = 0$ [$j = 1, 2, ..., N-1, N$] can be derived from $\gamma_4 = 0$.

B: The anomalous vanishment of the non-Hermitian skin effect for topologically nontrivial point gap

In the main text, we have exhibited that the non-Hermitian skin effect will be absent even though the point gap is topologically nontrivial, or equivalently, the spectral winding is a non-zero integer. This anomalous delocalization behavior of the eigenstates can be discussed more explicitly. Quantitatively, the non-Hermitian skin modes can be confirmed by the nonzero spectral winding $W = \frac{1}{2\pi i}\int_0^{2\pi} dk\partial_k \ln\det[H(k) - E_{ref}]$ [3] for a given base energy E_{ref}. For Bloch Hamiltonian $H(k)$ gained from Hamiltonian (S1), the residue theorem can be used to calculate the spectral windings through the replacement $e^{ik} = z$ and $dk = \frac{1}{iz}dz$. The spectral winding will have the form:

$$W = -\frac{1}{2\pi}\oint_{BZ} dz \frac{2\left((12+72i)z^4 + (34+80i)z^3 - (22+61i)z + (-8-32i)\right)}{z\left(2z^2 + (2-i)z + 2\right)\left((6+36i)z^2 + (10+47i)z + (4+16i)\right)}$$

for a given $E_{ref1} = 1 + \frac{1}{2}i$ for the given parameters [Fig. S2]. There exist five poles of order one on the complex plane: $z_1 = 0$, $z_2 = -\frac{2}{3} + \frac{1}{6}i$, $z_3 = -\frac{24}{37} - \frac{4}{37}i$, $z_4 = \frac{1}{4}\left((-2+i) + \sqrt{-13-4i}\right)$ and $z_5 = \frac{1}{4}\left((-2+i) - \sqrt{-13-4i}\right)$. It is clear that z_1, z_2, z_3 and z_4 are inside the unit circle, while z_5 is excluded, as shown in Fig. S3(a). Then, the residues from z_1 to z_4 are contributed to the spectral windings W, and finally $W = 1$. Visually, the spectral winding is equivalent to the curve defined as (Re[det[H(k)]], Im[det[H(k)]]). For our system, three eigenvalue branches in momentum space are $E_{k1} = V_a + t_a e^{-ik}$, $E_{k2} = V_c + t_c e^{ik}$ and $E_{k3} = V_b + 2t_b\cos(k)$ when $\gamma_1 = \gamma_4 = 0$. E_{k1} and E_{k2} will wind around in the clockwise and counterclockwise direction with k varying from 0 to 2π, respectively. Accordingly, as long as $V_a \neq V_c$ or $t_a \neq t_c$, there must exist a reference point E_{ref}, so that the number of circling around E_{ref} is just only once [we can here choose $E_{ref2} = 2 + 2i$], and W is not zero [4], as shown in Fig. S3(b). As such, the non-Hermitian skin effect should be existence.

However, this rule is not suitable when the unidirectional hopping amplitudes are considered. To understand the properties of the open boundary wavefunction more clearly, we go back to Eq. (S1) for $\gamma_1 = \gamma_4 = 0$, concretely, with $N = 3$. It can be found that

$$det\big[H_{OBC}-E_{OBC};3\times 3\big] =$$

$$\begin{pmatrix}
V_a-E_{OBC} & 0 & 0 & 0 & 0 & 0 & 0 & 0 & 0\\
\gamma_2 & V_b-E_{OBC} & \gamma_3 & 0 & t_b & 0 & 0 & 0 & 0\\
0 & 0 & V_c-E_{OBC} & 0 & 0 & t_c & 0 & 0 & 0\\
t_a & 0 & 0 & V_a-E_{OBC} & 0 & 0 & 0 & 0 & 0\\
0 & t_b & 0 & \gamma_2 & V_b-E_{OBC} & \gamma_3 & 0 & t_b & 0\\
0 & 0 & 0 & 0 & 0 & V_c-E_{OBC} & 0 & 0 & t_c\\
0 & 0 & 0 & t_a & 0 & 0 & V_a-E_{OBC} & 0 & 0\\
0 & 0 & 0 & 0 & t_b & 0 & \gamma_2 & V_b-E_{OBC} & \gamma_3\\
0 & 0 & 0 & 0 & 0 & 0 & 0 & 0 & V_c-E_{OBC}
\end{pmatrix}$$

$$= (V_a-E_{OBC})^3(V_c-E_{OBC})^3\begin{pmatrix} V_b-E_{OBC} & t_b & 0\\ t_b & V_b-E_{OBC} & t_b\\ 0 & t_b & V_b-E_{OBC}\end{pmatrix}. \tag{S16}$$

Hence, the three-band non-Hermitian system will be "simplified as" a Hermitian system when $\gamma_1=\gamma_4=0$, whose Hamiltonian is $H_B=t_b(C^{\dagger}{}_{B,n}C_{B,n+1}+C^{\dagger}{}_{B,n+1}C_{B,n})+V_bC^{\dagger}{}_{B,n}C_{B,n}$ [Fig. S3(c)]. In addition, we have analytically demonstrated that when $\gamma_1=\gamma_4=0$, there is no probability distribution on the A sub-chain and C sub-chain. Consequently, the distribution of the open boundary eigenstates of our non-Hermtian system is the distribution of the open boundary eigenstates of the reduced Hermitian system actually. To intuitively sense the localization behavior caused by the unidirectional hopping amplitudes, we plot the eigenstates corresponding to all eigenvalues in Fig. S3(d), where eigenstates have been normalized. It is clear that there is no extremely large number of eigenstates localized at the boundary of systems, i.e., the non-Hermitian skin effect is absent [Here, the information about the multifold exceptional points and the corresponding eigenstates is excluded because the Hamiltonian becomes defective in those points]. To confirm this, the inverse participation ratio (IPR) can be introduced as $IPR^s=\sum_{i=1}^{L}|\langle\Psi_i^s|\Psi_i^s\rangle|^2$ for the sth eigenstate $|\Psi^s\rangle$ [5]. Theoretically, IPR^s approaches zero for extended eigenstate, while it is finite for localized eigenstate in large system size. In Fig. S3(e), we numerically exhibit the open boundary eigenvalues with their unique IPR^s. Amazedly, one can easily see that the real eigenvalues are marked in a single color, i.e., $IPR^s\equiv 0.0037$ under numerical simulation. Thus, all eigenstates of our non-Hermitian system are extended, rather than localized. Namely, there not exists the non-Hermtian skin effect whereas the spectral winding number is a nonzero integer. In Figs. S3(f) and S3(g), we display the distribution of the eigenstates, which are indeed extended.

C: The anomalous emergence of the non-Hermitian skin effect for trivial point gap

As discussed above, the non-Hermitian skin effect can be vanishment even though the point gap is topologically nontrivial. So does the non-Hermitian skin effect have to disappear when the point gap is trivial? Based on previous works, the answer is in the affirmative. However, we can show that the rule will be also broken down. In order to obtain the trivial point gap, we restrict $V_a=V_c$, $t_a=t_c$, and $\gamma_1=\gamma_3=0$ for Hamiltonian. (S1), corresponding to the generalized Brillouin zone being a unit circle as well. Based on the definition,

$$W=-\frac{1}{2\pi}\oint_{BZ}dz\frac{(z^2-1)\left(E_{ref}^2z(t_b+t_c)-E_{ref}\left(2t_b\left(t_cz^2+t_c+V_cz\right)+t_cz(V_b+V_c)\right)+t_b\left(t_c^2z+2t_cV_c\left(z^2+1\right)+V_c^2z\right)+t_cV_bV_cz\right)}{z\left(z(E_{ref}-V_b)-t_b\left(z^2+1\right)\right)(-E_{ref}+t_cz+V_c)(z(V_c-E_{ref})+t_c)}$$

can be derived. Then, five poles of order one can be solved on the complex plane: $z_1=0$, $z_2=\frac{t_c}{E_{ref}-V_c}$, $z_3=\frac{E_{ref}-V_c}{tc}$, $z_4=\frac{\sqrt{E_{ref}^2-2E_{ref}V_b-4t_b^2+V_b^2}+E_{ref}-V_b}{2t_b}$ and $z_5=\frac{2t_b}{\sqrt{E_{ref}^2-2E_{ref}V_b-4t_b^2+V_b^2}+E_{ref}-V_b}$, i.e., $z_2z_3=1$ and $z_4z_5=1$. Only one of them is surrounded by the unit circle for z_2 (z_4) and z_3 (z_5) as long as $E_{ref}\neq V_c$, the schematics of which is shown in Fig. S4(a). Accordingly, three poles contribute to the definite integral and the spectral winding number $W=0$ is achieved. It seems that the non-Hermitian skin effect is lacking.

However, the IPR^s can be computed in Fig. S4(b). Obviously, it is finite for all eigenvalues, which implies that all open boundary eigenstates are localized. To accent the localization phenomena, all eigenstates as a function of the eigenvalues are revealed in Fig. S4(c) by exactly diagonalizing the open boundary Hamiltonian (S1). One can see that all eigenstates are indeed localized on the left boundaries of the system, rather than extended. Hence, the non-Hermitian skin effect is present unexpectedly even though the point gap is trivial.

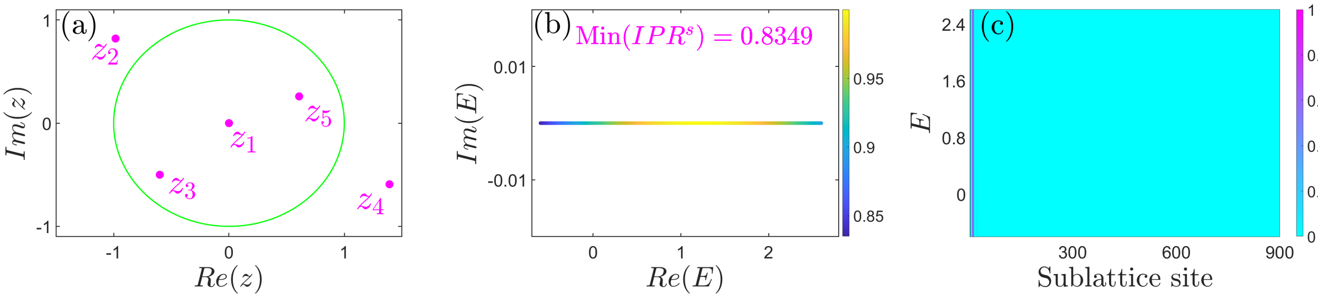

FIG. S4: (a) The sketch of the distribution of the poles about the spectral winding for a reference point E_{ref} on the complex plane, in which $z_1 = 0$ is in the unit circle, while if z_3 and z_5 are encircled, z_2 and z_4 must be excluded by the unit circle because of $z_2z_3 = z_4z_5 = 1$. Hence, the spectral winding number $W \equiv 0$ for any reference point. (b) The open boundary eigenvalues colored by their IPR^s, which are finite. (c) The normalized eigenstates as a function of eigenvalues, all of which are localized under open boundary conditions. The common parameters are $N = 300$, $\gamma_1 = \gamma_3 = 0$, $t_a = t_c = 6$, $t_b = \frac{4}{5}$, $\gamma_2 = 2$, $\gamma_4 = 1$, $V_a = V_c = \frac{6}{5}$, $V_b = 1$.

D: The mutations of the open boundary eigenvalues

We now analyze the properties of the open boundary energy spectrum when one of the elements of the set $\{\{\gamma_1, \gamma_3\}, \{\gamma_1, \gamma_4\}, \{\gamma_2, \gamma_3\}, \{\gamma_2, \gamma_4\}\}$ is zero. For example, the determinant $det[H_{OBC} - E_{OBC}; N \times N]$, when $\gamma_1 = \gamma_3 = 0$, has the form:

$$det\big[H_{OBC} - E_{OBC}; N \times N\big] = 0 =$$

$$\begin{pmatrix}
V_a - E_{OBC} & 0 & 0 & 0 & 0 & ... & 0 & 0 & 0 \\
\gamma_2 & V_b - E_{OBC} & 0 & 0 & t_b & ... & 0 & 0 & 0 \\
0 & \gamma_4 & V_c - E_{OBC} & 0 & 0 & ... & 0 & 0 & 0 \\
t_a & 0 & 0 & V_a - E_{OBC} & 0 & ... & 0 & 0 & 0 \\
0 & t_b & 0 & \gamma_2 & V_b - E_{OBC} & ... & 0 & 0 & 0 \\
. & . & . & . & . & ... & . & . & . \\
. & . & . & . & . & ... & . & . & . \\
. & . & . & . & . & ... & . & . & . \\
0 & 0 & 0 & 0 & 0 & 0\ .\ . & V_a - E_{OBC} & 0 & 0 \\
0 & 0 & 0 & 0 & 0 & 0\ .\ . & \gamma_2 & V_b - E_{OBC} & 0 \\
0 & 0 & 0 & 0 & 0 & 0\ .\ . & 0 & \gamma_4 & V_c - E_{OBC}
\end{pmatrix}, \tag{S17}$$

where N is the number of the unit cells. It can be found that the determinant satisfies a recurrence relation

$$det\big[H_{OBC} - E_{OBC}; N \times N\big] = a_1 det\big[H_{OBC} - E_{OBC}; N-1 \times N-1\big] - a_2 det\big[H_{OBC} - E_{OBC}; N-2 \times N-2\big], \tag{S18}$$

with $a_1 = (V_a - E_{OBC})(V_b - E_{OBC})(V_c - E_{OBC})$, $a_2 = (V_a - E_{OBC})^2(V_c - E_{OBC})^2 t_b^2$. Based on the recurrence relation, we have

$$det\big[H_{OBC} - E_{OBC}; N \times N\big] = \frac{2^{-N-1}\big[(a_1 + \sqrt{a_1^2 - 4a_2})^{N+1} - (a_1 - \sqrt{a_1^2 - 4a_2})^{N+1}\big]}{\sqrt{a_1^2 - 4a_2}} = 0. \tag{S19}$$

For simplicity, we set $a = a_1$ and $b = \sqrt{a_1^2 - 4a_2}$, As such Eq. (S19) can be formally written as

$$det\big[H_{OBC} - E_{OBC}; N \times N\big] = \frac{2^{-N-1}\big[(a+b)^{N+1} - (a-b)^{N+1}\big]}{b} = 0. \tag{S20}$$

Expand Eq. (S20) using the binomial theorem, and we can find

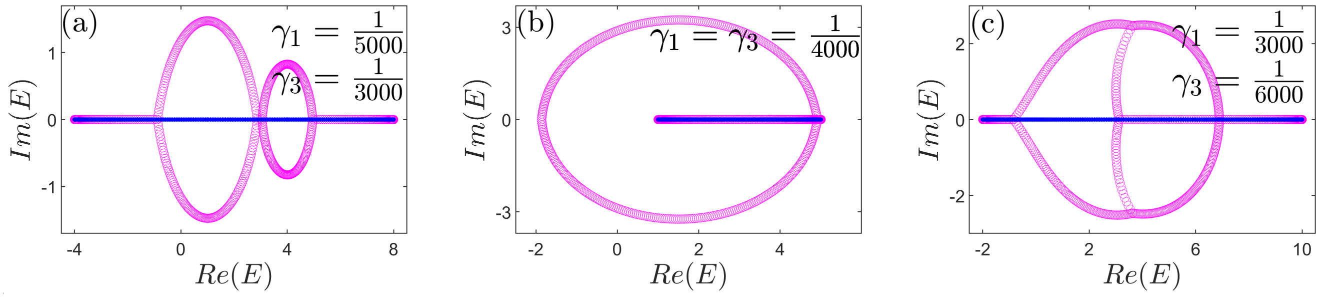

FIG. S5: (a) The open boundary energy spectrum with system size $N = 200$. The blue line laying on the real axis stands for the eigenvalues under $\gamma_1 = \gamma_3 = 0$. The distinction between the pink curve and the blue line shows that extremely small changes in parameters will result in mutations in the energy spectrum. The parameters are (a) $t_a = 2$, $t_b = 3$, $t_c = 1$, $\gamma_2 = \frac{1}{10}$, $\gamma_4 = \frac{1}{3}$, $V_a = 1$, $V_b = 2$ and $V_c = 4$. (b) $t_a = 3$, $t_b = 1$, $t_c = 4$, $\gamma_2 = \frac{1}{2}$, $\gamma_4 = 1$, $V_a = 2$, $V_b = 3$ and $V_c = 1$. (c) $t_a = 4$, $t_b = 3$, $t_c = 2$, $\gamma_2 = \frac{3}{2}$, $\gamma_4 = \frac{1}{4}$, $V_a = 3$, $V_b = 4$ and $V_c = 5$.

$$\frac{(a+b)^{N+1} - (a-b)^{N+1}}{b} = 2\big(C^1_{N+1}a^N b^0 + C^3_{N+1}a^{N-2}b^2 + C^5_{N+1}a^{N-4}b^4 + ...\big). \tag{S21}$$

Therefore, the determinant of the open boundary Hamiltonian is

$$det\big[H_{OBC} - E_{OBC}; N \times N\big] = 2^{-N}(V_a - E_{OBC})^N (V_c - E_{OBC})^N y(V_b, t_b, E_{OBC}) = 0, \tag{S22}$$

with

$$\begin{aligned} y(V_b, t_b, E_{OBC}) &= C^1_{N+1}(V_b - E_{OBC})^N + C^3_{N+1}(V_b - E_{OBC})^{N-2}\big[(V_b - E_{OBC})^2 - 4t_b^2\big] \\ &+ C^5_{N+1}(V_b - E_{OBC})^{N-4}\big[(V_b - E_{OBC})^2 - 4t_b^2\big]^2 + ... \end{aligned} \tag{S23}$$

Clearly, both $E_{OBC} = V_a$ and $E_{OBC} = V_c$ is the Nth-order exceptional point of the open boundary Hamiltonian with the system cell being N using the concept of the resultant [6, 7]. More importantly, we find that the polynomial $y(V_b, t_b, E_{OBC})$ is the determinant of the Hamiltonian $H_B = t_b(C^{\dagger}{}_{B,n}C_{B,n+1} + C^{\dagger}{}_{B,n+1}C_{B,n}) + V_b C^{\dagger}{}_{B,n}C_{B,n}$. Hence, the open boundary eigenvalues of the three-band system are $E_{OBC} = \{V_a, V_c, V_b + 2t_b cos(k)\}$ for $k \in \{\delta_k, 2\delta_k, ..., N\delta_k\}$ with $\delta_k = \frac{2\pi}{N}$. In other words, the energy spectrum under open boundary conditions must be the real numbers. However, after extensive numerical simulations, we find that as long as the subsystems are coupled, however weakly, the open boundary eigenvalues will be distributed on the complex plane. Namely, the extremely small changes in parameters will result in huge changes in the energy spectrum [Fig. S5].

E: The confirmation of "The inconsistency between the open boundary eigenvalues and the continuum bands"

In the main text, we have shown that the open boundary eigenvalues can not be reproduced by the continuum bands accompanied by the anomalous non-Hermitian skin effect. Now, we further confirm this singular situation analytically. We can review how to get the generalized Brillouin zone and the corresponding continuum bands from the characteristic polynomial $f(\beta, E)$ briefly: (i) choose a point β_0 arbitrarily in the complex number field; (ii) solve $f(\beta_0, E) = 0$, one of the roots marked as E_0; (iii) solve $f(\beta, E_0) = 0$, and order the roots by the absolute value; (iv) identify the ordering of two roots that have the same absolute values as $|\beta_0|$ [1,2,8]. For our system, if $|\beta_0| = |\beta_2(E_0)| = |\beta_3(E_0)|$, $\beta_2(E_0)$ and $\beta_3(E_0)$ are the elements of the generalized Brillouin zone and E_0 belongs to the corresponding continuum bands.

Based on those processes, we set the parameters as $\{t_a = t_c = \frac{11}{10}$, $t_b = \frac{6}{10}$, $\gamma_1 = \frac{1}{5}$, $\gamma_2 = \gamma_3 = 0$, $\gamma_4 = \frac{1}{10}$, $V_a = V_c = 1$, $V_b = \frac{6}{5}\}$ and $\beta_0 = e^{\frac{i\pi}{4}}$. Consequently, solving $f(\beta_0, E) = 0$, $E_{1,2} = 1 + \frac{11}{10}(\frac{\sqrt{2}}{2} \pm \frac{\sqrt{2}}{2}i)$, $E_3 = \frac{3}{5}(2 + \sqrt{2})$ are obtained. We can choose $E_0 = 1 + \frac{11}{10}(\frac{\sqrt{2}}{2} + \frac{\sqrt{2}}{2}i)$, and solve $f(\beta, E_0)$. The four solutions are

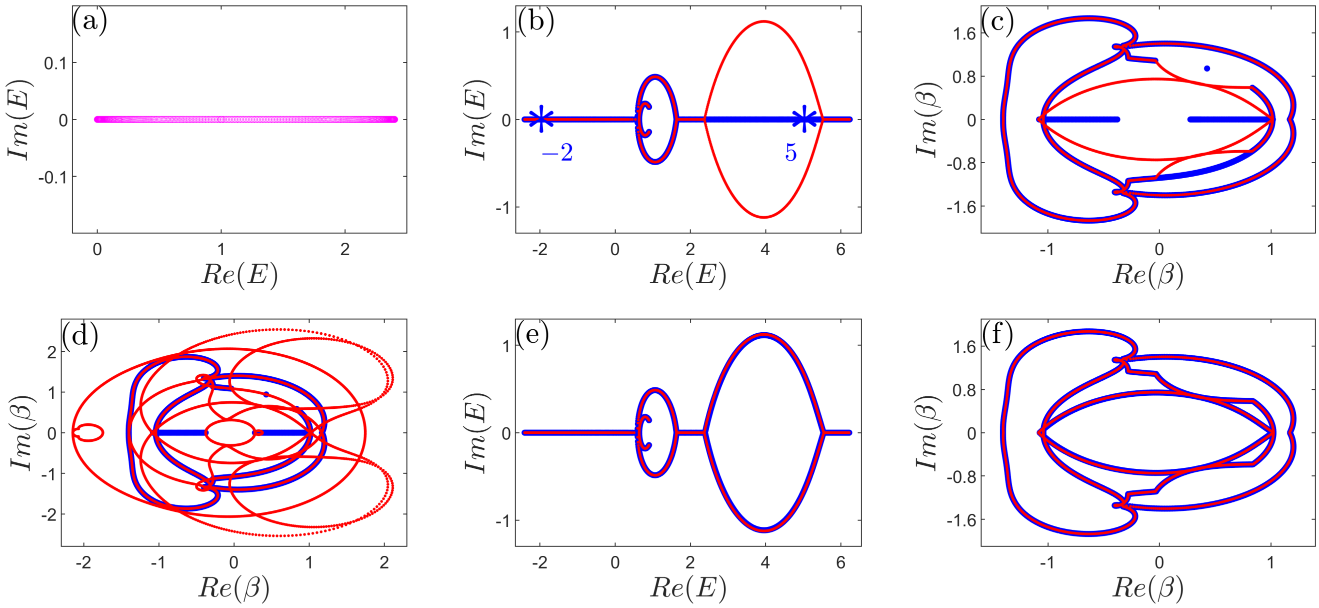

FIG. S6: (a) The open boundary structure, which lays on the real axis. The parameters are $N=300$, $\gamma_2=\gamma_3=0$, $t_a=t_c=\frac{11}{10}$, $t_b=\frac{3}{5}$, $\gamma_1=\frac{1}{5}$, $\gamma_4=\frac{1}{10}$, $V_a=V_c=1$, $V_b=\frac{6}{5}$. (b) and (e) The open boundary eigenvalues (the blue curve) and continuum bands (the red curve). (b) Two open boundary eigenvalues being selected. After bringing these two energy values into $f(\beta,E)$, one energy value obtain $|\beta_2|=|\beta_3|$ ($E_{OBC}=-2$) and the other corresponds to $|\beta_3|=|\beta_4|$ ($E_{OBC}=5$). (d) Auxiliary generalized Brillouin zone (the red curve), containing all information of $|\beta_m|=|\beta_n|$ with $f(\beta,E)=0$, and the generalized Brillouin zone obtained from the open boundary eigenvalues (the blue curve). (c) and (f) The generalized Brillouin zone gained from the open boundary eigenvalues (the blue curve) and the non-Bloch band theory (the red curve), respectively. For (b), (c) and (d) $\gamma_3=0$. For (e) and (f), $\gamma_3=\frac{1}{100}$. The common parameters from (b) to (f) are $N=700$, $t_a=1$, $t_b=2$, $t_c=\frac{3}{2}$, $\gamma_1=\frac{1}{2}$, $\gamma_2=2$, $\gamma_4=-1$, $V_a=1$, $V_b=2$ and $V_c=4$.

$$\begin{aligned}\{\beta_1(E_0),\beta_2(E_0),\beta_3(E_0),\beta_4(E_0)\}=\Big\{&\frac{1}{12}\left(-\sqrt{\left(11\sqrt[4]{-1}-2\right)^2-144}+11\sqrt[4]{-1}-2\right),\sqrt[4]{-1},-(-1)^{3/4},\\&\frac{1}{12}\left(\sqrt{\left(11\sqrt[4]{-1}-2\right)^2-144}+11\sqrt[4]{-1}-2\right)\Big\},\end{aligned}\tag{S24}$$

i.e.,

$$\{|\beta_1(E_0)|,|\beta_2(E_0)|,|\beta_3(E_0)|,|\beta_4(E_0)|\}=\{0.5185,1.000,1.000,1.928\}.\tag{S25}$$

Thus, $|\beta_0|$=$|\beta_2(E_0)|$=$|\beta_3(E_0)|$ for the given E_0, we can conclude that $\beta_2(E_0)$ and $\beta_3(E_0)$ are the ingredients of the generalized Brillouin zone, and E_0, a complex number, is included in the continuum bands. This result contradicts Fig. S6(a), where the open boundary eigenvalues are consistent with the real axis in those parameters.

We can also set $\beta_0=2e^{\frac{i\pi}{4}}$ and solve $f(\beta_0,E)=0$. Three solutions are $E_1=1+\frac{11}{5}e^{\frac{i\pi}{4}}$, $E_2=1-\frac{11}{20}e^{\frac{3i\pi}{4}}$ and $E_3=\frac{3}{10}(4+\sqrt{8+15i})$. E_0 can be chosen as $E_0=1+\frac{11}{5}e^{\frac{i\pi}{4}}$. $f(\beta,E_0)$ can be solved and the four solutions are

$$\begin{aligned}\{\beta_1(E_0),\beta_2(E_0),\beta_3(E_0),\beta_4(E_0)\}=\Big\{&\frac{1}{6}\left(-\sqrt{\left(11\sqrt[4]{-1}-1\right)^2-36}+11\sqrt[4]{-1}-1\right),-\frac{1}{2}(-1)^{3/4},2\sqrt[4]{-1},\\&\frac{1}{6}\left(\sqrt{\left(11\sqrt[4]{-1}-1\right)^2-36}+11\sqrt[4]{-1}-1\right)\Big\},\end{aligned}\tag{S26}$$

i.e.,

$$\{|\beta_1(E_0)|,|\beta_2(E_0)|,|\beta_3(E_0)|,|\beta_4(E_0)|\}=\{0.2848,0.5000,2.000,3.5113\}.\tag{S27}$$

Similarly, E_0 also can be chosen as $E_0 = E_2 = 1 - \frac{11}{20} e^{\frac{3i\pi}{4}}$, and $E_0 = E_3 = \frac{3}{10}(4 + \sqrt{8 + 15i})$. After calculation, one can obtain

$$\{|\beta_1(E_0)|, |\beta_2(E_0)|, |\beta_3(E_0)|, |\beta_4(E_0)|\}_{E_0=E_2} = \{0.5000, 0.7246, 1.380, 2.000\}, \tag{S28}$$

and

$$\{|\beta_1(E_0)|, |\beta_2(E_0)|, |\beta_3(E_0)|, |\beta_4(E_0)|\}_{E_0=E_3} = \{0.5000, 0.7789, 1.283, 2.000\}. \tag{S29}$$

Then, $\beta_0 = 2e^{\frac{i\pi}{4}}$ is not the ingredients of the generalized Brillouin zone, and E_1, E_2 and E_3 are not included in the continuum bands.

Next, we will transform our viewpoint, and analyze the singular phenomenon from another perspective. It is usually expected that when all open boundary eigenvalues are brought into the characteristic polynomial $f(\beta, E)$, and the second and third largest $|\beta|$ are selected, the obtained data should vest in the generalized Brillouin zone obtained from the non-Bloch band theory [1,2,8,9]. However, unlike the established scenarios, this fact is not suitable for the singular phenomenon. Specifically, we can arbitrarily choose some open boundary eigenvalues in Fig. S6(b), such as $E_{OBC} = -2$ and bring it into the characteristic polynomial $f(\beta, E)$. One can obtain

$$\begin{aligned}\{\beta_1, \beta_2, \beta_3, \beta_4\}_{E=-2} = \Big\{ &\frac{1}{18}\left(\sqrt[3]{11\left(18\sqrt{3}+31\right)} - \frac{11^{2/3}}{\sqrt[3]{18\sqrt{3}+31}} - 13\right), -\frac{1}{36}\left(1 - i\sqrt{3}\right)\sqrt[3]{11\left(18\sqrt{3}+31\right)} + \\ &\frac{11^{2/3}\left(1+i\sqrt{3}\right)}{36\sqrt[3]{18\sqrt{3}+31}} - \frac{13}{18}, -\frac{1}{36}\left(1 + i\sqrt{3}\right)\sqrt[3]{11\left(18\sqrt{3}+31\right)} + \frac{11^{2/3}\left(1-i\sqrt{3}\right)}{36\sqrt[3]{18\sqrt{3}+31}} - \frac{13}{18}, -4\Big\},\end{aligned} \tag{S30}$$

i.e.,

$$\{|\beta_1|, |\beta_2|, |\beta_3|, |\beta_4|\}_{E=-2} = \{0.3021, 1.050, 1.050, 4.000\}. \tag{S31}$$

Clearly, $|\beta_2| = |\beta_3|$. This equality also is the condition for obtaining the generalized Brillouin zone and the continuum bands. Namely, β_2 and β_3 are the elements of the generalized Brillouin zone, and $E_{OBC} = -2$ is the ingredient of the continuum band exactly.

Conversely, we choose another open boundary eigenvalue $E_{OBC} = 5$ and bring it into the characteristic polynomial $f(\beta, E)$. Accordingly,

$$\begin{aligned}\{\beta_1, \beta_2, \beta_3, \beta_4\}_{E=5} = \{ &\frac{1}{24}\left(\sqrt[3]{12\sqrt{16341} - 1223} - \frac{95}{\sqrt[3]{12\sqrt{16341} - 1223}} + 13\right), \frac{2}{3}, -\frac{1}{48}\left(1 - i\sqrt{3}\right)\sqrt[3]{12\sqrt{16341} - 1223} \\ &+ \frac{13}{24} + \frac{95\left(1+i\sqrt{3}\right)}{48\sqrt[3]{12\sqrt{16341} - 1223}}, \frac{95\left(1-i\sqrt{3}\right)}{48\sqrt[3]{12\sqrt{16341} - 1223}} - \frac{1}{48}\left(1 + i\sqrt{3}\right)\sqrt[3]{12\sqrt{16341} - 1223}\},\end{aligned} \tag{S32}$$

i.e.,

$$\{|\beta_1|, |\beta_2|, |\beta_3|, |\beta_4|\}_{E=5} = \{0.2397, 0.6667, 1.021, 1.021\}. \tag{S33}$$

Clearly, $|\beta_2| \neq |\beta_3|$, but $|\beta_3| = |\beta_4|$. This equality is not compatible with the condition of obtaining the generalized Brillouin zone and the continuum bands. In other words, when we exploit the condition $|\beta_2| = |\beta_3|$ to determine the continuum bands in the non-Bloch band theory, the results can only cover a part of the open boundary eigenvalues. This statement is visually confirmed in Fig. S6(b). In addition, we numerically plot the generalized Brillouin zone by bringing all open boundary eigenvalues into the characteristic polynomial $f(\beta, E)$, and selecting the second and third largest β. Meanwhile, the generalized Brillouin zone obtained from the non-Bloch band theory is exhibited in Fig. S6(c). One can see that the blue figure even has unclosed branches, whereas the red figure is closed on the complex plane. As such, when we rely on the non-Bloch band theory, the obtained continuum bands and the open boundary eigenvalues will exist wide variations.

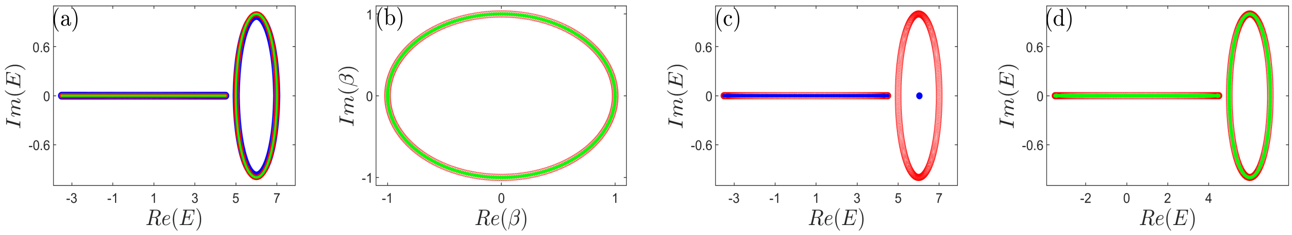

FIG. S7: (a) The energy spectra under open boundary (the blue curve) and periodic boundary conditions (the green curve) and the continuum bands (the red curve) with $\gamma_1 = \frac{\gamma_3}{2} = \frac{1}{1000}$. (b) The Brillouin zone (the green curve) and the generalized Brillouin zone (the red curve). (c) The open boundary eigenvalues (the blue curve) and the continuum bands (the red curve). Meanwhile, an open boundary eigenvalue is separated, which is the multifold exceptional point. (d) The eigenvalues obtained from the momentum space (the green curve) and the continuum bands (the red curve). For (b), (c) and (d), $\gamma_1 = \gamma_3 = 0$. The common parameters are $N = 400$, $t_a = t_c = 1$, $t_b = 2$, $\gamma_2 = 2\gamma_4 = \frac{1}{2}$, $V_a = V_c = 6$ and $V_b = \frac{1}{2}$.

The singular behavior of the open boundary eigenvalues also can be confirmed from a general view of the auxiliary generalized Brillouin zone [8]. Ref. [8] has demonstrated that the auxiliary generalized Brillouin zone can be obtained by solving $f(\beta, E) = 0$ with E traverses the entire complex number field, and extracting $|\beta_m| = |\beta_n|$, ($\{m, n\} = \{1, 2, 3, 4\}$). Therefore, the generalized Brillouin zone is the subset of the auxiliary generalized Brillouin zone. However, despite the auxiliary generalized Brillouin zone possessing all information of $f(\beta, E) = 0$, some blue data points, especially those on the real axis, still can not be recovered in Fig. S6(d). Namely, the singular open boundary spectrum even can not be obtained from the auxiliary generalized Brillouin zone, let alone the generalized Brillouin zone. However, if the parameters of the system were changed slightly, from $\gamma_3 = 0$ to $\gamma_3 = \frac{1}{100}$. The open boundary eigenvalues will have mutations. Correspondingly, the generalized Brillouin zone obtained from two different methods also coincides together, as shown in Figs. S6(e) and S6(f).

F: The irrelevance between singular open boundary eigenvalues and the generalized Brillouin zone

We can further show that the singular phenomenon of the eigenvalues is not accompanied by the change of the generalized Brillouin zone. To confirm this, we restrict that the generalized Brillouin zone is a unit circle [$t_a = t_c$, $V_a = V_c$ and $\gamma_1\gamma_2 = \gamma_3\gamma_4$]. Normally, the eigenvalues under open boundary and periodic boundary conditions, and the continuum bands are consistent with each other, as shown in Fig. S7(a) with $\gamma_1 = \frac{\gamma_3}{2} = \frac{1}{1000}$ [also discussed in Fig. S2(b)]. However, the situations will have remarkable mutations when $\gamma_1 = \gamma_3 = 0$, corresponding to unidirectional hopping of B sub-chain and A sub-chain, B sub-chain and C sub-chain. As shown in Fig. S7(b), the generalized Brillouin zone remains the unit circle. Correspondingly, there is very little change for the continuum bands, while the open boundary eigenvalues instead will produce mutations and fall on the real axis entirely in Fig. S7(c). Namely, the open boundary energy structure and the continuum bands can not match each other. Importantly, we can analytically show that the multifold exceptional points [the blue dot encircled by the red curve in Fig. S7(c)] can not be overlapped by the continuum bands in this case. In addition, the continuum bands are still consistent with the periodic boundary eigenvalues in Fig. S7(d), which means that the open boundary and periodic boundary eigenvalues are paradoxical with each other whereas the generalized Brillouin zone is a unit circle.

The consistency between periodic boundary eigenvalues and the continuum band can be shown analytically. On the one hand, we have exhibited that the energy spectrum of the momentum space when $t_a = t_c$, $V_a = V_c$ and $\gamma_1 = \gamma_3 = 0$, are $E_{1,2} = V_a + t_a e^{\pm ik}$, $E_3 = V_b + 2t_b\cos(k)$. On the other hand, the characteristic polynomial of our system has the form:

$$f(\beta, E) = \det[H(\beta) - E] = \frac{\big(-\beta E + \beta^2 t_b + t_b + \beta V_b\big)\big(-E + \beta t_a + V_a\big)\big(\beta(V_a - E) + t_a\big)}{\beta^2} = 0. \tag{S34}$$

The corresponding four roots are

$$\beta_1 = \frac{E - V_b - \sqrt{E^2 - 4t_b^2 - 2EV_b + V_b^2}}{2t_b}, \beta_2 = \frac{t_a}{E - V_a}, \beta_3 = \frac{E - V_a}{t_a}, \beta_4 = \frac{E - V_b + \sqrt{E^2 - 4t_b^2 - 2EV_b + V_b^2}}{2t_b}.$$

Next, we bring $E_1 = V_a + t_a e^{ik}$ into these solutions and find that $\beta_2 = e^{-ik}$ and $\beta_3 = e^{ik}$, i.e., $|\beta_2| = |\beta_3| = 1$. Thus, $E_1 = V_a + t_a e^{ik}$ is the part the continuum bands. Similarly, $E_2 = V_c + t_c e^{-ik}$ and $E_3 = V_b + 2t_b\cos(k)$ are

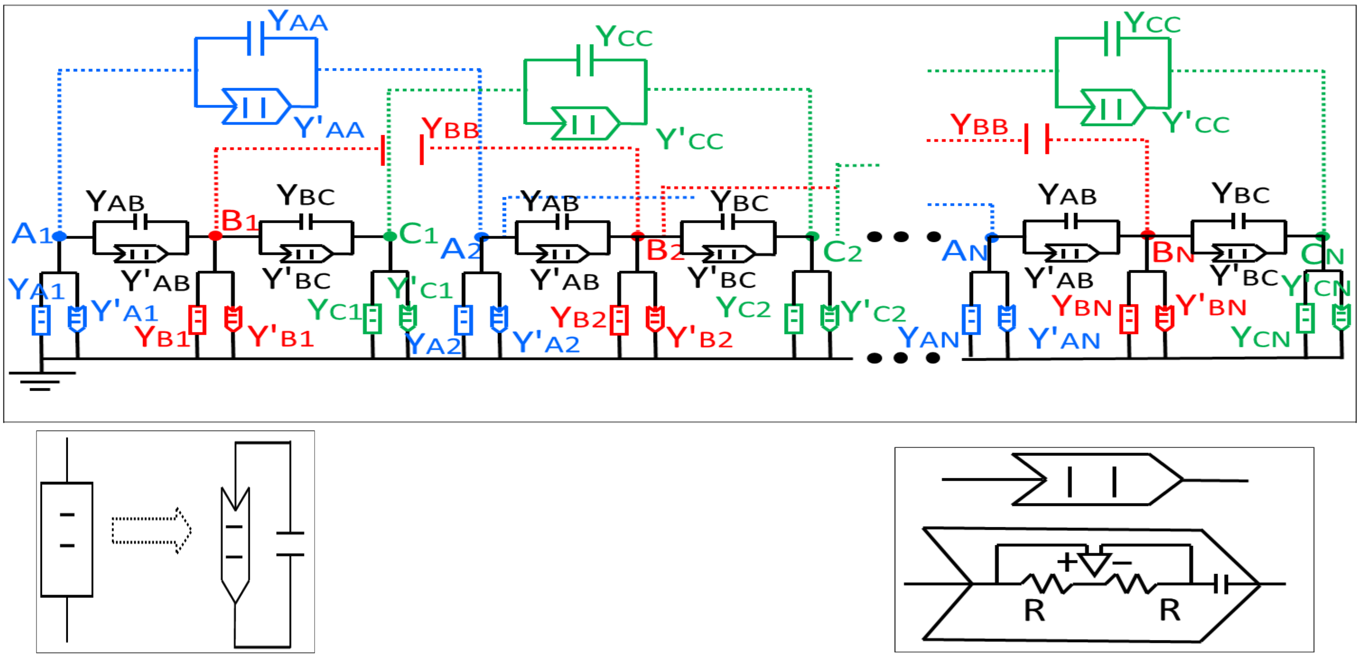

FIG. S8: Upper panel: the configuration of the electric circuit to simulate Hamiltonian (S1). Y_{AA}, Y_{BB} and Y_{CC} are the capacitance of the capacitor. Y'_{AA} and Y'_{CC} are the capacitance of the INIC for a capacitor. A-subchain, B-subchain and C-subchain are respectively connect by those electric devices. Y_{AB} and Y'_{AB} being respectively the capacitance of the capacitor and INIC for a capacitor connect the A-subchain and B-subchain, while Y_{BC} and Y'_{BC} connect the B-subchain and C-subchain. The on-site potential is obtained by grounding each node with suitable circuit devices. Lower panel: the structure of the INIC.

the part of the continuum bands. Then, the energy spectrum of the momentum space is the subset of the continuum bands, i.e., $E_{PBC} \subseteq E_{\infty}$. Next, we can solve Eq. (S34) again with respect to E, and the solutions are $E_1 = V_c + t_c\beta$, $E_2 = \frac{t_a+V_a\beta}{\beta}$, $E_3 = \frac{t_b+V_b\beta+t_b\beta^2}{\beta}$. As we have shown above, the generalized Brillouin zone has the form $\beta = e^{ik}$. Accordingly, the continuum bands will simplify as $E_{1,2} = V_a + t_a e^{\pm ik}$, $E_3 = V_b + 2t_b\cos(k)$, i.e., $E_{\infty} \subseteq E_{PBC}$. As such, the continuum bands and the periodic boundary eigenvalues are the same as with others exactly, which are distributed on the complex plane. The consistency between the periodic boundary eigenvalues and the continuum bands also reflects the paradox between the open boundary eigenvalues and the continuum bands.

We can further discuss the exceptional point when the generalized Brillouin zone is a unit circle. On the one hand, we have shown that $E = V_a$ and $E = V_c$ must belong to the open boundary eigenvalues as long as one of the elements of the set $\{\{\gamma_1,\gamma_3\},\{\gamma_1,\gamma_4\},\{\gamma_2,\gamma_3\},\{\gamma_2,\gamma_4\}\}$ is zero, which has no matter with t_a, t_b and t_c. On the other hand, $E = V_c + t_c e^{\pm ik}$ belong to the continuum bands exactly. Therefore, $E = V_a$ and $E = V_c$ can not be reproduced by the continuum bands except for $t_c = 0$. Moreover, the presence or absence of $E = V_b$ on the open boundary structure depends on the size of the system. Yet, $E = V_b + 2t_b\cos(k)$ belongs to the continuum bands as well, which means that $E = V_b$ must present on the continuum bands with $k = \frac{\pi}{2}$.

IV: The experimental realization in electric circuits

As shown above, the "Singular eigenstate localization and energy spectrum induced by the unidirectional hopping" has been elucidated theoretically. So far, there exist several physical configurations that can be used to demonstrate the non-Hermitian systems, including the cold atoms, electrical circuits, photonic and acoustic systems. Among them, electric circuits have been widely used to analyze the non-Hermitian properties because the circuit structure can be flexibly designed to facilitate integration and mass production. Here, we propose a possible experimental scheme by employing circuits to simulate the Hamiltonian (S1), as shown in Fig. S8. The basic properties of circuit systems are described by Ohm's law and Kirchhoff's law. According to those two laws, we have $I = JV$, where the components of the column vector I and V correspond respectively to the current and voltage of each node. Hence, the circuit Laplacian J can be used to simulate the Hamiltonian. In addition, we note that the impedance of the negative impedance converter with current inversion (INIC) [10, 11] will be changed from positive to negative if the

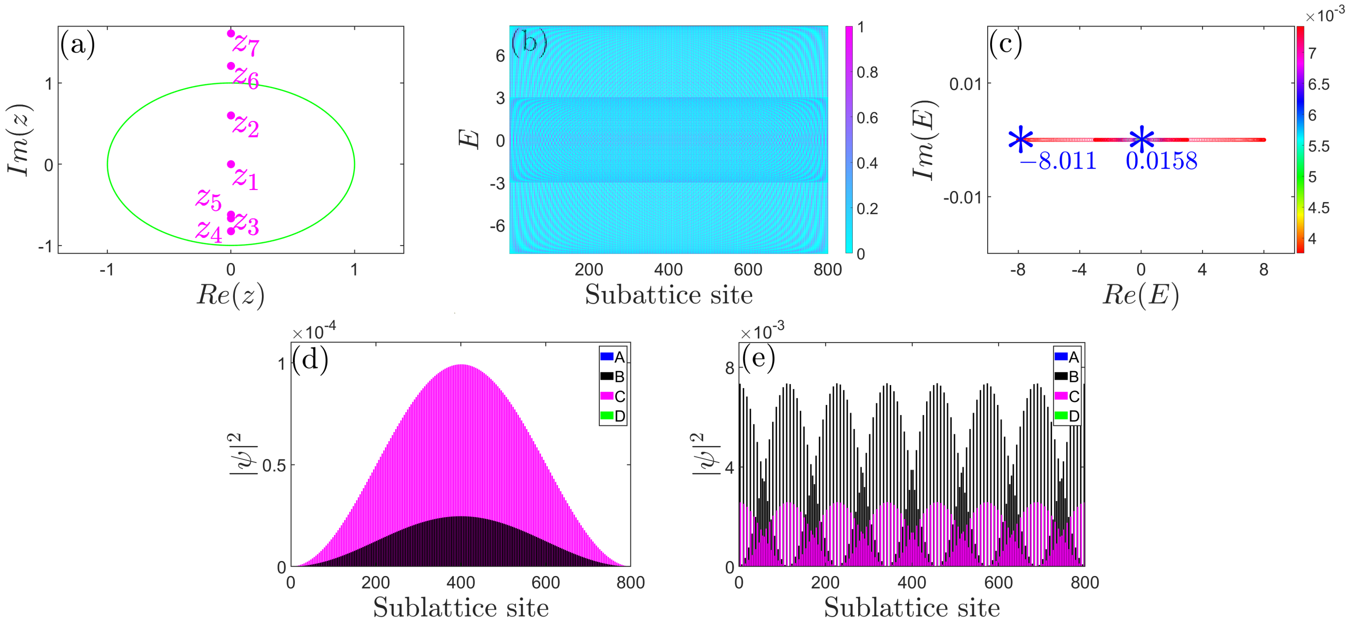

FIG. S9: (a) The distribution of all poles about the expression of the spectral windings on the complex plane, in which z_1, z_2, z_3 and z_4 and z_5 are surrounded by the unit circle, while z_6 and z_7 are outside the unit circle for a reference point $E_{ref} = \frac{3}{2}i$. (b) The open boundary eigenvalues colored by their respective IPR^s, the number of which approaches zero. (c) and (d) The distribution of the open boundary eigenstate corresponding to two eigenvalues in (b), in which only the occupation on B sub-chain and C sub-chain is non-zero, while A sub-chain and D sub-chain have no occupation. The common parameters are $N = 200$, $\gamma_1 = \gamma_6 = 0$, $t_a = 1$, $t_b = \frac{3}{2}$, $t_c = 4$, $t_d = \frac{5}{2}$, $\gamma_2 = \frac{1}{2}$, $\gamma_3 = \frac{1}{4}$, $\gamma_4 = \gamma_3$ and $\gamma_5 = \frac{1}{10}$.

current orientation through the device is reversed. Consequently, the nonreciprocal hoppings can be simulated by the combination of the capacitor and INIC. Further, the on-site potential is realized by grounding each node with appropriate parameters of the electric devices. Finally, to establish the mapping between circuits systems and our Hamiltonian (S1), we will take $Y_{A1} = V_a$, $Y_{Aj} = V_a + t_a$ $(1 < j \le N)$, $Y^{'}_{Aj} = -\gamma_1$, $Y_{AB} = -\frac{\gamma_1+\gamma_2}{2}$, $Y^{'}_{AB} = \frac{\gamma_1-\gamma_2}{2}$, $Y_{AA} = Y^{'}_{AA} = -\frac{t_a}{2}$, $Y_{B1} = Y_{BN} = V_b$, $Y_{Bj} = V_b + t_b$ $(1 < j < N)$, $Y_{BC} = -\frac{\gamma_3+\gamma_4}{2}$, $Y^{'}_{BC} = \frac{\gamma_3-\gamma_4}{2}$, $Y_{BB} = -t_b$, $Y_{Cj} = V_c$ $(1 \le j < N)$, $Y_{CN} = V_c - t_c$, $Y^{'}_{Cj} = -(\gamma_4 + t_c)$, $Y_{CC} = -\frac{t_c}{2}$ and $Y^{'}_{CC} = \frac{t_c}{2}$. The energy spectrum is obtained from the admittance spectrum of the circuit.

V: Anomalous non-Hermitian skin effect in four-band system

We have shown that the anomalous non-Hermitian skin effect can be induced by the unidirectional hopping based on a concrete three-band non-Hermitian system. Actually, the results can be generalized to other systems, such as the four-band non-Hermitian system, the Hamiltonian of which is

$$\begin{aligned} H_4 = \sum_{n=1}^{N} \Big[& t_a C^{\dagger}{}_{A,n+1} C_{A,n} + t_d C^{\dagger}{}_{D,n} C_{D,n+1} + t_b (C^{\dagger}{}_{B,n} C_{B,n+1} + C^{\dagger}{}_{B,n+1} C_{B,n}) + t_c (C^{\dagger}{}_{C,n} C_{C,n+1} + C^{\dagger}{}_{C,n+1} C_{C,n}) \\ & + \gamma_1 C^{\dagger}{}_{A,n} C_{B,n} + \gamma_2 C^{\dagger}{}_{B,n} C_{A,n} + \gamma_3 C^{\dagger}{}_{B,n} C_{C,n} + \gamma_4 C^{\dagger}{}_{C,n} C_{B,n} + \gamma_5 C^{\dagger}{}_{C,n} C_{D,n} + \gamma_6 C^{\dagger}{}_{D,n} C_{D,n} \Big], \end{aligned} \tag{S35}$$

where $C^{\dagger}{}_{j,n}$ and $C_{j,n}$ represent the creation and annihilation operators for sublattice j $(j = A, B, C, D)$ in n-th unit cells, respectively. t_a (t_b, t_c, t_d) is the hopping amplitudes for the the sub-chain A (B, C, D). γ_1 and γ_2 are hopping parameters between A and B sub-chain. γ_3 and γ_4 are hopping parameters between B and C sub-chain. Meanwhile, γ_5 and γ_6 are hopping parameters between C and D sub-chain. The on-site potential is not considered without loss of generality.

For Hamiltonian (S35), the spectral winding $W = \frac{1}{2\pi i} \int_0^{2\pi} dk \partial_k \ln \det[H_4(k) - E_{ref}]$ [3] for a base energy E_{ref} also

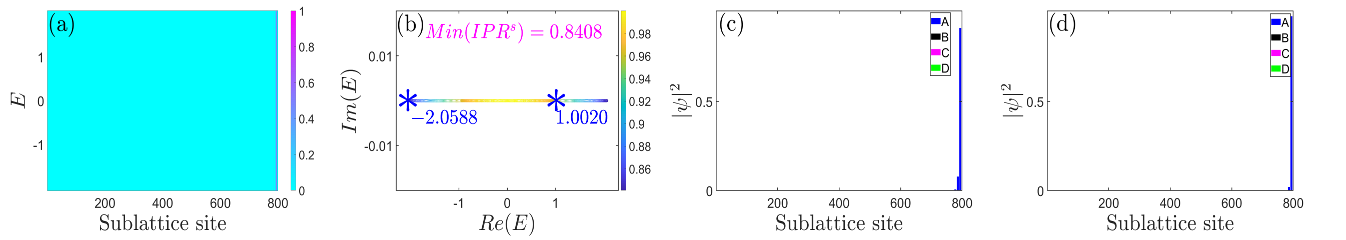

FIG. S10: (a) The open boundary eigenvalues colored by their respective IPR^s, the number of which approaches to zero. (b)The open boundary energy spectrum with the corresponding IPR^s, whose value is finite. (c) and (d) Amplitudes of two open boundary eigenstates corresponding to two eigenvalues in (b), which are localized at the boundaries. The common parameters are $N = 400$, $\gamma_2 = \gamma_6 = 0$, $t_a = t_d = 7$, $t_b = \frac{1}{2}$, $t_c = 1$, $\gamma_1 = \frac{1}{2}$, $\gamma_3 = \frac{1}{4}$, $\gamma_4 = \gamma_3$ and $\gamma_5 = \frac{1}{10}$.

can be evaluated through the residue theorem via replacing $e^{ik} = z$ and $dk = \frac{1}{iz}dz$. Explicitly,

$$W = -\frac{1}{2\pi}\oint_{BZ} \frac{3\left(2160z^6 - 1884iz^5 + 1519z^4 - 1252z^2 + 696iz - 864\right)}{z\left(2160z^6 - 2826iz^5 + 4557z^4 - 3925iz^3 + 3756z^2 - 1044iz + 864\right)}dz$$

is obtained for a given $E_{ref} = \frac{3}{2}i$, and seven poles of order one are derived:

$$z_1 = 0, z_2 = \frac{3}{5}i, z_3 = -\frac{2}{3}i, z_4 = -\frac{1}{96}\left(\sqrt{209} + 48\sqrt{\frac{5257}{1152} - \frac{11\sqrt{209}}{384}} - 33\right)i,$$

$$z_5 = \frac{1}{96}\left(\sqrt{209} - \sqrt{2\left(33\sqrt{209} + 5257\right)} + 33\right)i, z_6 = -\frac{1}{96}\left(\sqrt{209} - 48\sqrt{\frac{5257}{1152} - \frac{11\sqrt{209}}{384}} - 33\right)i$$

and

$$z_7 = \frac{1}{96}\left(\sqrt{209} + \sqrt{2\left(33\sqrt{209} + 5257\right)} + 33\right)i.$$

As shown in Fig. S9(a), z_1, z_2, z_3, z_4 and z_5 is encircled by the unit circle, while z_6 and z_7 is outside. Finally, the spectral winding $W = 1$ is received and the non-Hermitian skin modes are existence conventionally. However, if we exhibit the distribution of all eigenstates in Fig. S9(b), the images intuitively shows that most of the eigenstates are not localized at the boundary. Further, the localization properties for the sth eigenstate $|\Psi^s\rangle$ also can be examined from the perspective of IPR^s [5]. As shown in Fig. S9(c), all numbers of IPR^s approach zero, i.e., all open boundary eigenstates are extended, rather than localized. Thus, the non-Hermitian skin effect is vanishment even though the winding number is a non-zero quantum integer. In Figs. S9(d) and S9(e), two eigenstates are displayed, both of which are extended in the non-Hermitian system.

Now, we exhibit the appearance of the non-Hermitian skin effect whereas the point gap is topologically trivial($W \equiv 0$). To satisfy this equation, the conditions can be limited as $t_a = t_d$ and $\gamma_2 = \gamma_6 = 0$ in Fig. S10. In fact, those conditions make the generalized Brillouin zone a unit circle ideally for Hamiltonian (S35). In this case, the number of the poles of the spectral winding are $z_1 = 0$, $z_3 = \frac{1}{z_2}$, $z_5 = \frac{1}{z_4}$ and $z_7 = \frac{1}{z_6}$, i.e., a total of four poles contribute to the spectral winding, and $W \equiv 0$ is obtained. It is then generally believed that the non-Hermitian skin effect is lacked. Yet, the distribution of all eigenstates also illustrates that most of the open boundary eigenstates are localized at the system boundaries [Fig. S10 (a)]. Furthermore, the localized behavior of the eigenstates can be easily inferred from the energy spectrum and the associated IPR^s in Fig. S10 (b). In Figs. S10 (c) and S10 (d), the open boundary eigenstates are indeed localized at the boundaries.

* Electronic address: tanlei@lzu.edu.cn
† Electronic address: wliu@iphy.ac.cn

[1] S. Yao and Z. Wang, Phys. Rev. Lett. **121**, 086803 (2018), URL https://link.aps.org/doi/10.1103/PhysRevLett.121.086803.
[2] K. Yokomizo and S. Murakami, Phys. Rev. Lett. **123**, 066404 (2019), URL https://link.aps.org/doi/10.1103/PhysRevLett.123.066404.
[3] N. Okuma, K. Kawabata, K. Shiozaki, and M. Sato, Phys. Rev. Lett. **124**, 086801 (2020), URL https://link.aps.org/doi/10.1103/PhysRevLett.124.086801.
[4] Y. Yi and Z. Yang, Phys. Rev. Lett. **125**, 186802 (2020), URL https://link.aps.org/doi/10.1103/PhysRevLett.125.186802.
[5] X. Li, X. Li, and S. Das Sarma, Phys. Rev. B **96**, 085119 (2017), URL https://link.aps.org/doi/10.1103/PhysRevB.96.085119.
[6] P. Delplace, T. Yoshida, and Y. Hatsugai, Phys. Rev. Lett. **127**, 186602 (2021), URL https://link.aps.org/doi/10.1103/PhysRevLett.127.186602.
[7] E. J. Bergholtz, J. C. Budich, and F. K. Kunst, Rev. Mod. Phys. **93**, 015005 (2021), URL https://link.aps.org/doi/10.1103/RevModPhys.93.015005.
[8] Z. Yang, K. Zhang, C. Fang, and J. Hu, Phys. Rev. Lett. **125**, 226402 (2020), URL https://link.aps.org/doi/10.1103/PhysRevLett.125.226402.
[9] K. Yokomizo and S. Murakami, Progress of Theoretical and Experimental Physics **2020** (2020), ISSN 2050-3911, 12A102, https://academic.oup.com/ptep/article-pdf/2020/12/12A102/35611788/ptaa140.pdf, URL https://doi.org/10.1093/ptep/ptaa140.
[10] Q.-B. Zeng and Y. Xu, Phys. Rev. Research **2**, 033052 (2020), URL https://link.aps.org/doi/10.1103/PhysRevResearch.2.033052.
[11] T. Helbig, T. Hofmann, S. Imhof, M. Abdelghany, T. Kiessling, L. W. Molenkamp, C. H. Lee, A. Szameit, M. Greiter, and R. Thomale, Nature Physics **16**, 747 (2020), ISSN 1745-2481, URL https://doi.org/10.1038/s41567-020-0922-9.